

Hybrid Circulating Current Control of a Modular Multilevel Converter for Primary Frequency Response Support

J. LAPSLEY
University of Manitoba
Canada

S. FILIZADEH
University of Manitoba
Canada

X. SHI
RTDS Technologies
Canada

SUMMARY

This paper investigates the use of modular multilevel converters (MMCs) for primary frequency support through the extension of the active power capability of the converter into an overload region. When the converter enters the overload region, which is required for providing short-term frequency support, a specialized circulating-current control system injects a characteristic second-harmonic dominated current into the converter arms while dynamically limiting the arm current in order to prevent any violations of the semiconductor specifications. A novel, hybrid approach to the circulating current control scheme provides maximum power with a fast initial response after the occurrence of a frequency event and then switches to droop control after the frequency has recovered to a user-defined threshold. This combination grants optimal support for a large rate of change of frequency (RoCoF) and the ability to manage different infeed losses. The proposed controller is verified on a generic network within the PSCAD/EMTDC environment.

KEYWORDS

Renewable energy, HVDC, VSC, MMC, inertia emulation, power systems
umlapsle@myumanitoba.ca

I. INTRODUCTION

The modern power system is evolving. Influences stemming from changing fuel prices, laws and regulations have resulted in a rise in renewable energy generation [1]. Often, the best sites for harnessing renewable wind and solar energy are in remote locations, far away from load centres and grid infrastructure. In order to maximize efficiency, these renewable sources are commonly connected to the power grid through the use of voltage source converter-high voltage direct current (VSC-HVDC) transmission technologies [2].

To produce the robust frequency that is required for the ac power system and synchronous machine stability and security, generation and consumption are required to be in balance [3] (Note that this is true in conventional power systems wherein storage of energy is either unavailable or does not meet dynamic requirements). Therefore, a direct consequence of an increase in the renewable generation penetration is the reduction in conventional synchronous machine generation, which also implies a reduction in system inertia. The large amount of inertia provided by synchronous machines has historically been the main mechanism for primary frequency control. Solar and wind energy, connected to the power system via VSC-HVDC is electromagnetically decoupled from the network, and hence, no physical inertia is provided from these sources [4]. This results in a shift from a conventional, inertia rich, synchronous machine-based power system, to a modern, inertia deficient, converter-based power system.

Currently, the solutions put into practice to strengthen a low inertia power system are to ensure a minimum number of synchronous machines are in service or the installation of synchronous condensers at predetermined buses [4]. However, as the penetration of renewable sources and VSCs continues to grow, it becomes logical for converters to be tasked to also provide emulated inertia required for frequency control ancillary services (FCAS) [1]. In order for a converter to participate in FCAS while operating at its rated values, it must be able to safely provide additional power in excess of the rated power, effectively operating in an overload region.

The converter commonly used in modern VSC-HVDC transmission is the modular multilevel converter (MMC). As seen in Figure 1, the MMC consists of six arms, each one comprised of a series connected submodule string. The submodule is commonly implemented in a half-bridge arrangement, composed of a capacitor and two switches with anti-parallel diodes. The operation of the MMC is based on the control of the switches in each submodule, either inserting or bypassing the voltage across that module's capacitor. This action is done in such a way that the desired ac and dc voltages at the points of connection (POCs) of the converter are produced [5].

The main limitation of extending the power range of the MMC is found in the IGBT switches. IGBTs are sensitive to over-current failures and must be operated in a physically imposed safe operating area (SOA). Pushing the IGBT outside the limits of the SOA runs the additional risk of thermal breakdown. One option to reach the overload region is through oversizing the IGBTs. Alternatively, the overload region can be reached, without significant increases in IGBT ratings, by manipulating the circulating current through the arms in such a way that the peak arm current is reduced to within the bounds of the SOA [6]. The circulating current is internal to MMC and does not leave the converter [5]. Operating the MMC continuously in such a fashion will increase the steady state losses; however, under emergency situations such as FCAS this could be acceptable.

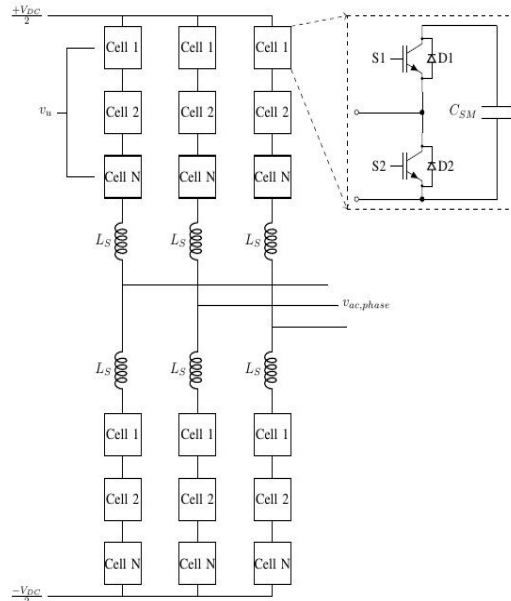


Figure 1 : The topology of a half bridge MMC.

This paper builds on the research presented in [6] which makes use of two methods, maximum power control and droop control for the operation of an MMC in an overload region. This paper furthers this concept by presenting a hybrid controller with a fast-initial response to a frequency event, to minimize the rate of change of frequency (RoCoF), and the ability to handle different infeed losses efficiently. The effectiveness of the proposed controller is measured on a generic power system.

II. INERTIA

The imbalance between mechanical and electric torques during a frequency event in a synchronous machine can be approximated by the swing equation,

$$J\omega_m \frac{d\omega_m}{dt} = P_{gen} - P_{load} \quad (1)$$

where J is the combined moment of inertia of the generator and turbine in $kg \cdot m^2$, ω_m is the angular velocity of the rotor in rad/s (which at steady state is the same as the system angular frequency), P_{gen} is the generated power dictated by the mechanical torque and P_{load} is the power demand dictated by the electromagnetic torque.

The swing equation can be normalized by making use of the per unit inertia constant, H . H is defined as the kinetic energy in W/s at rated speed, normalized to the VA_{base} of the generator. The H constant indicates how long, in seconds, a generator is able to provide its rated power at the rated frequency.

$$H = \frac{1}{2} \frac{J\omega_{0m}^2}{VA_{base}} \quad (2)$$

Rearranging this equation and substituting it into (1) yields,

$$2H \frac{d\omega_{g,pu}}{dt} = P_{gen,pu} - P_{load,pu} \quad (3)$$

where the subscript pu denotes per unit. As the angular velocity is in per unit, (3) can be rewritten in terms of frequency as,

$$\frac{2H}{f} \frac{df}{dt} = P_{gen,pu} - P_{load,pu} \quad (4)$$

where f is the rated system frequency and df/dt is the RoCoF [3]. As renewable generation is added and synchronous machines are decommissioned the inertia of the power system decreases, which in turn increases the RoCoF within the same time frame. Large RoCoFs are undesirable as they interfere with timing mechanisms in synchronous generation control systems and phase locked loops (PLLs) in renewable generation. This can lead to the incorrect operation of protection and in the worst-case scenarios, cascaded black outs [4]. Therefore, the power system requires an additional source of inertia. In this paper a specific control scheme is implemented within the converter.

Inertia is directly linked to a power system's ability to resist change. The larger the inertia the more difficult it is to change the frequency of a power system. Since, synchronous machines are coupled to the power system, the delivery of inertia during a frequency event is executed instantaneously and without the need of a control system. Renewable generation, in the form of wind and photovoltaics, are decoupled from the power system and hence have a reduced amount or complete absence of inertia.

The virtual inertia implemented in the hybrid controller of this paper is of the fast frequency response (FFR) type [7]. The inertia is not implemented instantaneously, as it is in synchronous machines, because the detection time of the frequency event needs to be taken into consideration. Also, the decoupled nature of renewable generation means there is no stored kinetic energy. The requested power from renewable generation is increased and used to balance the swing equation. The renewable generation(s) in question must not be already operating at rated power output. Adding this term into (4) yields,

$$\frac{2H}{f} \frac{df}{dt} = P_{gen,pu} - P_{load,pu} + P_{RES,virtual} \quad (5)$$

In (5) $P_{RES,virtual}$ is the additional power delivered from renewable generation for the purposes of limiting the nadir, reducing the RoCoF and ensuring the system is able to reach a new stable operating point.

III. MMC CCSC

To minimize losses that stem from circulating currents within the arms of the converter, MMCs are commonly equipped with a circulating current suppression control (CCSC). CCSC is implemented using a Park transformation to transform the 3-phase circulating currents into two dc currents, consisting of the d and q components. PI-controllers drive the d and q components to the set reference values ($I_{cir,d}$ and $I_{cir,q}$), which are zero in the case for CCSC [8].

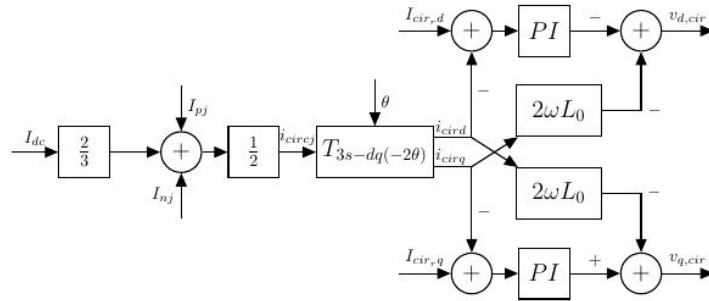


Figure 2: Block diagram of the CCSC control scheme.

The hybrid controller presented in this paper is implemented using the same control method as CCSC. The reference values for the d and q components of current remain zero when the hybrid controller is inactive. When the hybrid controller detects a frequency deviation signal, the d and q current references are automatically set accordingly.

IV. HYBRID CONTROLLER

The hybrid controller follows the frequency and is activated when the frequency falls below a user defined threshold as seen in Figure 3. This controller makes use of two control philosophies: a maximum power controller is implemented for the purpose of reducing the nadir, and RoCoF during the inertial period. After the inertial period, a proportional droop controller maintains varying infeed losses until system protection controls are able to change power set points such that the system returns to nominal frequency.

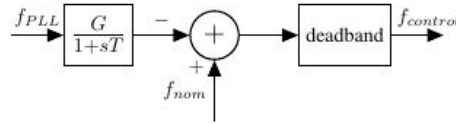


Figure 3: Frequency signal that is used for detection of power imbalance.

A. Power Controller

In this section, the concept of overload is introduced and the method of implementing that into the controller is presented.

1) *Overload:* To provide system support via an HVDC link, using an MMC operating at its rated capacity under the assumption that the switches are not significantly oversized, the MMC must have a control system that allows it to operate outside of its rated capacity, in an overload region. The limits of the P/Q operating capability of the MMC are imposed by four main factors: the peak arm current, the peak submodule voltage, the arm voltage capability, and the overmodulation ability of the MMC [6]. Of these four, this work focuses on increasing the limit of the peak arm current. The peak arm current is imposed by the peak current that the IGBTs can safely and reliably switch while remaining in the SOA. Pushing current greater than this limit through IGBTs can cause failure due to thermal breakdown or latch up [9]. This limit can be increased through techniques like the one found in [10], where 2nd harmonic current is injected into the MMC arms in such a way that it reduces the peak

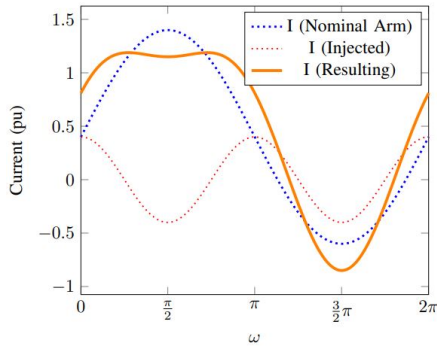


Figure 4: General method of reducing the peak of the arm current through means of injecting 2nd harmonic current.

arm current to an acceptable level that does not violate the SOA of the IGBTs. A general example of how the 2nd harmonic current is able to reduce the peak of the arm current is shown in Figure 4.

arm current to an acceptable level that does not violate the SOA of the IGBTs. A general example of how the 2nd harmonic current is able to reduce the peak of the arm current is shown in Figure 4.

2) *Maximum Power Controller:* To create a fast initial response to counter large RoCoFs, this works considers the use of injecting a 2nd harmonic dominated controlled circulating current into the arms of the MMC. This reduces the peak of the arm current to a level within the bounds of the SOA of the IGBT for the purpose of maximizing the amount of overload capacity. As in [10], by using the injected circulating current (i_{inj}) in (6), a 25% overload above the rated power limit of the MMC is achieved.

$$i_{inj} = I_{inj} \sin(2\omega t' + \varphi_{inj}) \quad (6)$$

The values for I_{inj} and φ_{inj} are derived based on the derivative of the arm current. This produces a piecewise solution that is programmed into the control block of Figure 5. The resulting magnitude and phase of the required 2nd harmonic current ($i_{cir,rd}$ and $i_{cir,rq}$) are fed as the new reference values for the CCSC (Figure 2).

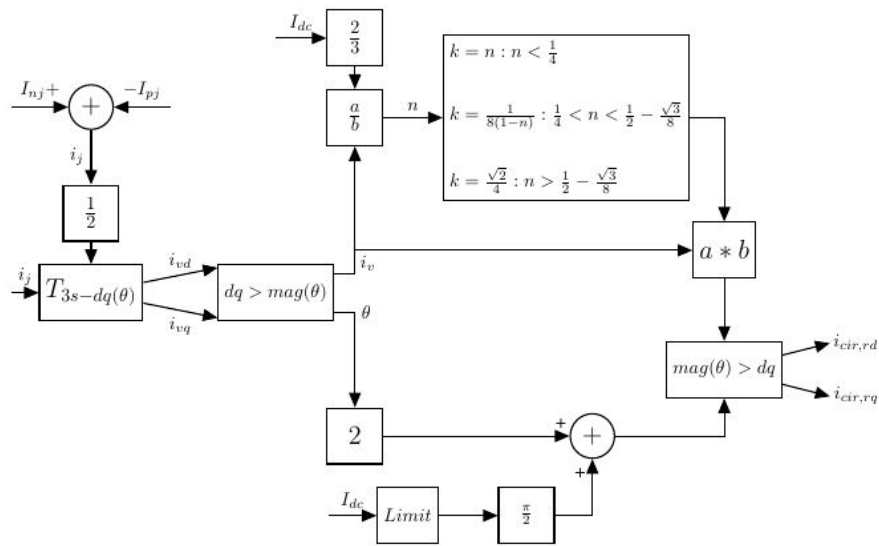


Figure 5: Block diagram of the maximum power control scheme.

B. Droop Controller

After the inertial period, where the RoCoF is minimized by the maximum power controller, the 2nd harmonic current injected into the arm is altered for the purposes of controlling infeed losses until the power system's frequency controls are able to resolve the imbalance. The relationship between the amplitude of the injected 2nd harmonic current, the phase of the injected 2nd harmonic current and the peak of the arm current is recorded from simulations using a modulation index of 0.8, and presented in Figure 6. Figure 7 shows that if the phase of the injected 2nd harmonic current is kept constant and the amplitude of the injected 2nd harmonic current is decreased, a linear relationship emerges. Through extensive simulations this linearity is found to be consistent for different modulating indices. Therefore, this relationship is used to implement a proportional droop controller. The proportional overload support ranges from a maximum of 25% above the rated power limit of the MMC, in line with the maximum power controller, to a minimum of rated power, that coincides with CCSC.

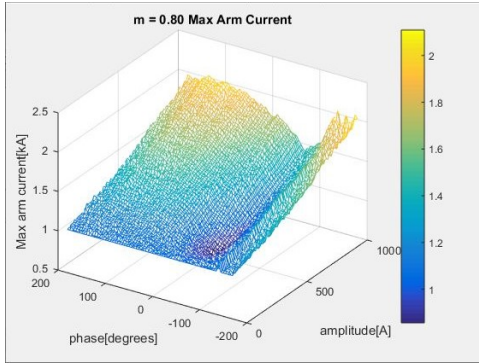


Figure 6: The behaviour of peak arm current as the phase and magnitude of the 2nd harmonic current is varied.

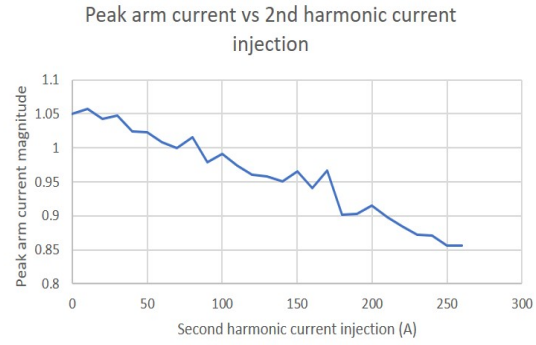


Figure 7: Peak arm current with the phase of the 2nd harmonic current kept constant while varying the magnitude of the 2nd harmonic current.

The proportional droop control implementation is shown in Figure 8. Here, the droop is a user defined parameter.

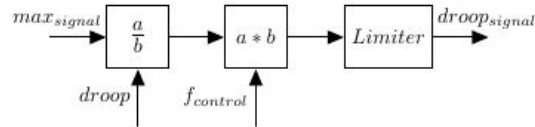


Figure 8: Proportional droop controller.

V. TEST NETWORK

Two tests are done to validate the operation of the controller. The test system specifications are presented in Table I. A single-mass synchronous machine model is implemented in PSCAD-EMTDC for the purpose of simulating the inertial response and frequency control capabilities of the hybrid controller. The rotating masses of all the synchronous machines that link to conventional generation are lumped together as a single synchronous machine. The governor controls act solely on this single mass. In using this model, the frequency control dynamics are focused on, while other aspects of the power system, such as voltage variations and electromechanical oscillations can be neglected [11].

The MMC connects to an ideal dc voltage source. This simulates an HVDC interconnector where any amount of power can be delivered. This simulation does not take into account limitations such as HVDC link overload.

An active load of 120 MW is switched in at 30s using a circuit breaker to create a controlled power imbalance. The inertia constant of the synchronous generator varies from 5.2s to 1.2s (in steps of 1s) to simulate a progressively weaker system.

TABLE I
SYSTEM PARAMETERS

Synchronous Machine & Coupling Transformer Specifications				
Frequency: 60Hz	Voltage: 18kV	H :1.2s - 5.2s	Rating:600MVA, 370kV/230kV	$X_{leakage}$: 10%
Converter & Converter Transformer Specifications				
SMs/Arm : 76	C_{cell} : 2800 μF	L_{arm} : 50mH	Rating:600MVA, 370kV/230kV	$X_{leakage}$: 10%
System Specifications				
DC Voltage = 640kV		MMC POC SCR = 3		MMC X/R ratio = 5

VI. SIMULATION RESULTS

To verify effectiveness for the proposed controller two tests are simulated. The synchronous generator in this model has two operation modes. In one mode, the generator supplies the required amount of power to the grid. This is dictated by how much power the HVDC link is supplying to the loads. Here, the HVDC link, controlled by the MMC, is held constant.

The other operation mode allows control of the active and reactive power references of the synchronous generator. Using this mode, the power reference of the synchronous generator is held constant and the proposed controller in the MMC compensates for the power imbalance via the HVDC link. Five seconds after introducing the power imbalance, the power reference of the synchronous generator increases to simulate the system protection controls. The proposed MMC controls reduce the power delivered by the HVDC link in the same proportion that the synchronous generator increases power. When the MMC is safely operating at the original set point, CCSC control can take over.

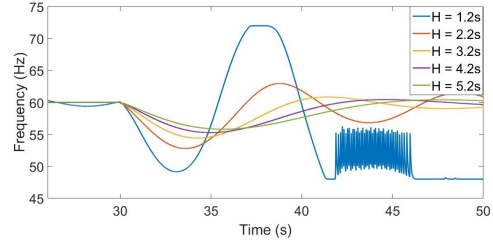


Figure 9: Frequency response of the synchronous generator with the proposed MMC controller disabled.

A. Test 1: DC link power constant, power imbalance rectified by synchronous machine.

Five simulations are done at different inertia constants to demonstrate the behaviour of the system with the proposed MMC control disabled. The synchronous generator solely reacts to correct the power imbalance that is introduced. The frequency response of the synchronous generator is displayed in Figure 9.

Decreasing the inertia constant in the synchronous machine reduces the ability of the generator to resist changes in frequency. This manifests as an increase in RoCoF, a more pronounced nadir, a faster reaction, and a decrease in stability. When the inertia constant is set to 1.2s in this simulation, the generator becomes unstable.

B. Test 2: DC link power controlled by MMC, power imbalance rectified by synchronous machine after 35s.

Five simulations are done to show the behavior of the proposed MMC control. The inertia constant of the synchronous machine is changed for each simulation from 5.2s to 1.2s. The power imbalance is met with virtual inertia by means of the MMC controlled HVDC link. This happens

180ms after the power imbalance is introduced. At 35s the power reference of the synchronous machine increases to simulate system protection controls. The set point increases the synchronous generator power such that it can correct the power imbalance. This allows the HVDC link power to

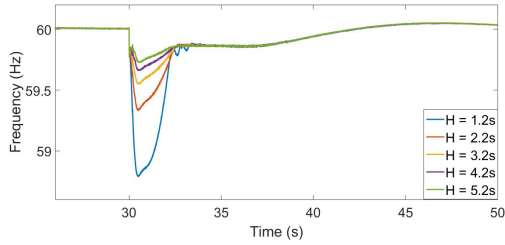


Figure 10: Frequency response of the synchronous generator with the proposed MMC controller enabled.

decrease to its pre-disturbance value. The frequency response is displayed in Figure 10.

As the inertia constant is decreased there is an increase in RoCoF and nadir; however, the overall reaction time increases as compared to test 1, as does the stability. The use of the proposed controller ensures that even low inertia constants, such as 1.2s, are stable.

Looking closer at the worst-case scenario ($H = 1.2s$) in Figure 11. The decrease in synchronous machine frequency (a), is not initially corrected by the inertia stored in the synchronous machine (b); rather, it is met with

an increase in power delivered from the HVDC link (c). To ensure that IGBT switches do not operate in the SOA a judicious amount of circulating current is injected into the MMC ((d), (e)).

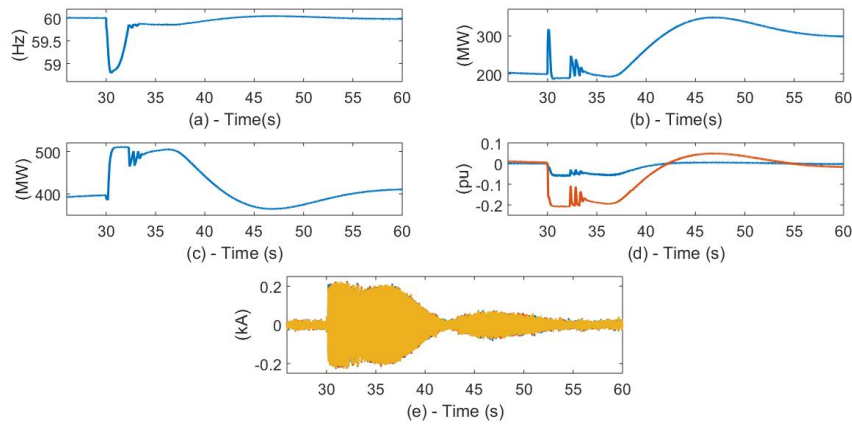


Figure 11: System response with proposed controller enabled, $H = 1.2s$, (a) frequency of synchronous generator, (b) active power delivered from synchronous generator, (c) active power delivered via HVDC link, (d) I_d (orange) and I_q (blue) of the circulating current, (e) three phase circulating current

The upper and lower arm currents of a single-phase leg of the MMC are shown in Figure 12. Prior to the power imbalance the MMC operates in CCSC control. The arm current in Figure 12 (28s – 28.04s) shows that the circulating current is close to zero. CCSC control is used until a frequency deviation is detected. A delay time of 180ms is used to register the detection at which point the maximum power controller is enabled. The controls enter the maximum power control mode. This transition from CCSC to maximum power control is seen in Figure 12 (30.14s – 30.22s). In this control mode the MMC is delivering the maximum amount of additional power while obeying the SOA of the IGBTs. In order for this to happen, judicious amounts of circulating current are injected into each arm of the MMC as seen in Figure 11 (e). This reduces the peak of the arm current such that the SOA of the IGBTs is obeyed, as seen at 30.24s – 30.28s in Figure 12. As the synchronous machine begins to increase to another operating point, the power delivered by the HVDC link, controlled by the MMC, begins reducing. At this point the controller switches to the proportional droop control. The amount of circulating current required to safely operate at this point reduces and the arm current takes a form unlike pure CCSC or maximum power as seen in Figure 12 (38.54s – 38.58s). Finally, the HVDC link returns to its rated power output and the controller switches back to CCSC control as seen in Figure 12 (59.96s – 60s).

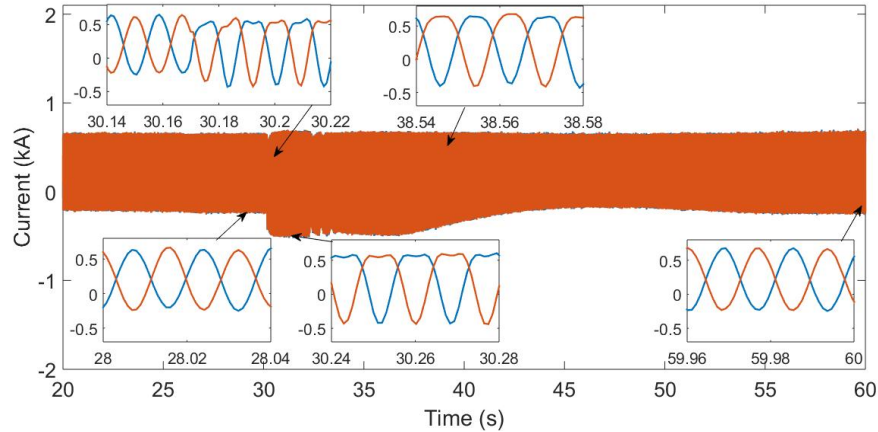


Figure 12: Phase A, top and bottom arm current of the MMC with proposed controller enabled, $H = 1.2s$.

VII. CONCLUSION

Emulation of inertia was achieved by injecting circulating currents into the arms of the MMC. The maximum power controller is able to meet a power imbalance, significantly reducing the nadir of the frequency. The linear relationship that exists when the amplitude of the of the 2nd harmonic current is reduced while keeping the phase of the 2nd harmonic current constant, allows the controller to react effectively to different infeed losses. The paper validated the proposed MMC controller performance through extensive electromagnetic transient simulation studies of a test system and showed that there is significant improvement in frequency response in terms of nadir, RoCoF and stability, especially in scenarios of very lower synchronous machine inertia.

BIBLIOGRAPHY

- [1] U. Tamrakar, D. Shrestha, M. Maharjan, B. Bhattarai, T. Hansen, and R. Tonkoski, "Virtual inertia: Current trends and future directions," vol. Vol.7, no. 7, p. p.654, 2017.
- [2] D. V. Hertem, O. Gomis-Bellmunt, and J. Liang, *HVDC Grids: For Offshore and Supergrid of the Future*. WileyIEEE Press, 2016.
- [3] P. Kundur, *Power System Stability and Control*. McGrawHill, Inc., 1994.
- [4] H. Gu, R. Yan, and T. Saha, "Review of system strength and inertia requirements for the national electricity market of australia," vol. Vol.5, no. 3, pp. p.295–305, 2019.
- [5] K. Sharifabadi, L. Harnefors, H. P. Nee, S. Norrga, and R. Teodorescu, *Design, control and application of modular multilevel converters for HVDC transmission systems*. John Wiley and Sons, Incorporated, 2016.
- [6] I. M. Sanz, P. D. Judge, C. E. Spallarossa, B. Chaudhuri, and T. C. Green, "Dynamic overload capability of vsc hvdc interconnections for frequency support," vol. Vol.32, no. 4, pp. p.1544–1553, 2017.
- [7] "Australian, Energy, Market, and Operator", "Fast frequency response in the nem," 2017.
- [8] A. The, B. Freudenberg, S. Dieckerhoff, V. Vahrenholt, W. Fischer, R. Stornowski, and M. Wildmann, "Operation range of hvdc-mmc with circulating current suppression and energy balancing control," pp. p.1–9, 2015.
- [9] P. D. Judge and T. C. Green, "Dynamic thermal rating of a modular multilevel converter hvdc link with overload capacity," 2015.
- [10] Z. Lianghe, S. Chao, L. Qifu, L. Pandian, Z. Hongqi, and H. Tao, "Research on new circulating current control strategy for increasing the power transmission capacity of modular multilevel converter," 2018. [2]D. V. Hertem, O. Gomis-Bellmunt, and J. Liang, *HVDC Grids: For Offshore and Supergrid of the Future*. WileyIEEE Press, 2016.
- [11] A. Adamczyk, M. Altin, Omer G " oksu, R. Teodorescu, " and F. Iov, "Generic 12-bus test system for wind power integration studies," 2013